Quantification of Rotational Thallium-201 Myocardial Tomography

Ernest V. Garcia, Kenneth Van Train, Jamshid Maddahi, Florence Prigent, John Friedman, Joseph Areeda, Alan Waxman, and Daniel S. Berman

Cedars-Sinai Medical Center, and University of California, Los Angeles, California

A comprehensive method is described for quantification of the relative 3-dimensional distribution of Tl-201 in the myocardium, following stress and subsequent washout. The method uses maximal-count circumferential profiles of well-defined long- and short-axis tomograms to determine the 3-dimensional distribution of Tl-201; it then maps this distribution onto a 2-dimensional polar representation. Abnormal thallium distribution or washout is identified by automatic computer comparison of each patient's profile with the corresponding lower limits of normal profiles. Abnormality is expressed as a percentage of the entire myocardium by use of polar maps for extent and severity. The binary extent map states whether a given location is normal or abnormal, and the severity map expresses the degree of abnormality. Preliminary criteria for abnormality were derived from the tomographic results of 25 normals and 28 patients with documented coronary artery disease. The results were normal in 23 of the 25 normals and were abnormal in 25 of the 28 CAD patients. In addition, the computer output correctly localized the presence or absence of disease in 46 of 56 coronary circulations.

J Nucl Med 26:17–26, 1985

Rotational myocardial tomography after injection of thallium-201 at peak exercise has been suggested as a significant improvement over planar scintigraphy for the detection and localization of myocardial ischemia (*1–4*). Rotational thallium-201 tomography at rest has also been reported to be better than planar imaging for the detection and localization of myocardial infarction (*5–7*), as well as for estimations of the extent of the infarct (*6,7*). Despite increasing availability of methods for quantifying planar Tl-201 myocardial scintigraphy (*8–12*), current evaluation of regional myocardial perfusion from stress/redistribution rotational tomography is usually made by visual interpretation of the reconstructed Tl-201 tomograms. This approach is limited by observer variability, inability to account for differences in regional photon attenuation, inability to assess myocardial washout, inability to quantify the percentage of the myocardium that is involved with either a perfusion defect or a washout abnormality, and the time-consuming procedure of visually assessing approximately 20 to 40 tomograms.

Previously we developed and validated a comprehensive computerized method that uses sequential planar stress/redistribution scintigraphy to express objectively, as a function of space and time, the relative distribution of Tl-201 in the myocardium (*8*). Using the attributes of this planar approach, we have developed a comprehensive method that quantifies the three-dimensional distribution of myocardial Tl-201 at stress and redistribution from rotational tomograms. This approach expresses the percentage of the myocardium involved with a perfusion defect and/or washout abnormality. The purpose of this report is to describe the method and to evaluate its preliminary results in normal patients and in patients with coronary artery disease (CAD).

METHODS

Patient selection

Two groups of patients were studied. Group A consisted of 25 patients referred to this institution for assessment of suspected CAD, but who were classified as

Received Mar. 28, 1984; revision accepted Aug. 1, 1984.

For reprints contact: Ernest V. Garcia, PhD, Dept. of Nuclear Medicine, Cedars-Sinai Medical Ctr., Box 48750, Los Angeles, CA 90048.

normal by probability analysis. This group included 19 males and six females ranging in age from 28 to 70 yr (mean 46 yr). These patients were considered as normals by having less than 5% likelihood of CAD as judged by sequential Bayesian analysis of age, sex, symptom classification, and the results of the exercise electrocardiogram and fluoroscopic assessment of coronary calcification (*13*). Group B consisted of 28 consecutive patients with no electrocardiographic evidence of prior myocardial infarction, who underwent both Tl-201 rotational tomography and coronary angiography, and whose arteriographic studies revealed greater than 50% luminal stenosis of at least one of the three major coronary arteries. This group included 24 males and four females ranging in age from 35 to 78 yr (mean 61 yr). Twenty patients had disease of the anterior coronary circulation corresponding to the territory supplied by the left anterior descending coronary artery (LAD), and 22 had disease of the posterior coronary circulation corresponding to the territory supplied by the left circumflex (LCX) and the right coronary arteries (RCA). Fourteen of these patients had disease involving both anterior and posterior circulations.

Exercise and scintigraphic procedure

Patients in Groups A and B underwent stress and redistribution Tl-201 rotational tomography. They were stressed using multistage treadmill exercise according to the Bruce protocol. Exercise was maximal, terminated only after the patient developed chest pain, exhaustion, serious arrhythmia, or hypotension. A dose of 2 mCi of Tl-201 was injected at maximum exercise, and the patients continued to exercise for 45–90 sec after injection. At approximately 6 min, and again at 3–6 hr after injection of Tl-201, the patients were imaged using a rotating camera tomographic unit. Thirty-two projections were obtained for 30 sec each in an 180° arc extending from the 45° right anterior oblique to the left posterior oblique projection. The large-field-of-view scintillation camera was equipped with 75 photomultiplier tubes, a 0.25-in.-thick NaI(Tl) crystal and a low-energy, all-purpose, parallel-hole collimator. A 20% energy window was centered on the 80-keV x-ray peak. All projections were stored on magnetic disk using a 64 × 64, 16-bit matrix.

Computer processing and analysis

Each of the 32 projections was corrected for nonuniformity with a cobalt-57 source, collecting 30 million counts. The mechanical center of rotation was determined from the projection data to align the detector data with respect to the reconstruction matrix. The center-of-rotation measurement was also used periodically to monitor gantry stability (*14*). Filtered backprojection was then performed using a low-resolution Hanning filter with a cutoff frequency of 0.375 cycles/pixel to reconstruct the transverse axial tomograms (of 5.6 mm each) encompassing the entire heart. These tomograms were then smoothed in depth using a three-point weighted average with weighting factors of 1, 2, and 1, respectively. Sagittal and oblique tomograms parallel to the long and short axes of the left ventricle were extracted from the filtered transaxial tomograms by performing a coordinate transformation with appropriate interpolation (*15*). Algorithms for both the filtered backprojection and the coordinate transformation used were available in the commercial computer system used for this analysis. All tomograms were corrected to reflect the change in counts between stress and delayed imaging by using multiplicative scale factors provided by the commercial programs. The need for this correction arises because transaxial tomograms are normalized so that the maximum reconstructed pixel value does not overflow. Thus the extracted values need correction in order to provide the count change between the stress and delayed studies. No attenuation or scatter correction was used.

Three-dimensional quantification

Using the long-axis slice with the largest cavity length, the operator selected the short-axis cuts for quantification to extend from three cuts (16.8 mm) from the base of the left ventricle (LV) to the endocardial aspect of the apex (Fig. 1). On the short-axis cut falling halfway between apex and base, the operator then defined the center of the ventricular cavity, radius of search, and the inferior junction between right ventricle (RV) and LV as an anatomic landmark, which was arbitrarily aligned to the 102° arc. The maximal-count circumferential profiles (CPs) for each short-axis cut were then generated automatically from the most apical to the most basal cut. Each point in these profiles represents the maximum

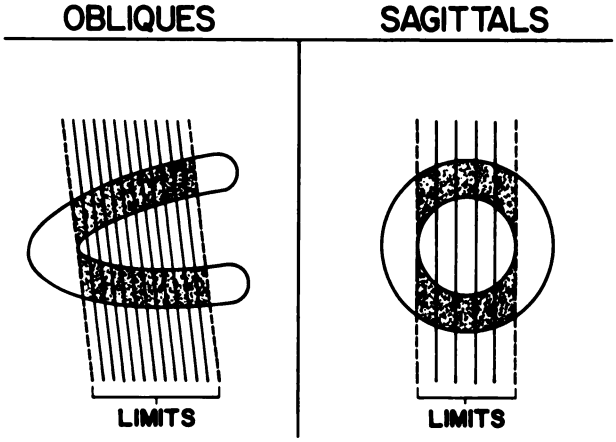

FIGURE 1
Diagram of method of slice selection used to circumvent partial-volume effect for both short-axis or oblique cuts (left) and long-axis or sagittal cuts (right). Left ventricle is usually divided into 9–12 short-axis cuts and 4–6 long-axis cuts. Each cut is 5.6 mm thick

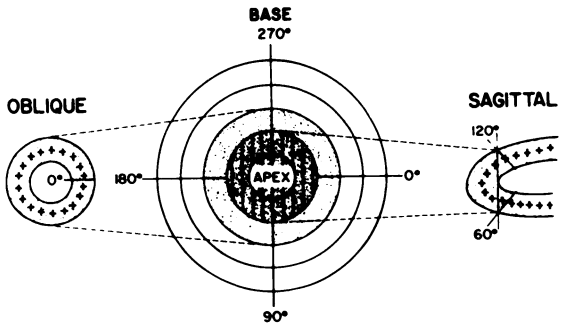

FIGURE 2
Diagram to show how three-dimensional information, as determined from oblique and sagittal circumferential profiles, is mapped onto a two-dimensional plane

counts per pixel along a radius extending from the center of the LV to the limit of the radius of search. The profile was constructed by the computer from the values of 60 radii spaced at 6° intervals plotted clockwise. Each profile was normalized to the maximum pixel value found for that profile. The same procedure, similarly automated, was then repeated for the long-axis cuts. Using the short-axis slice with the largest cavity diameter, the operator selected the long-axis cuts to be quantified as those ranging from the endocardial aspects of the septal wall to the endocardial aspect of the lateral wall (Fig. 1). The operator then defined, on the long-axis cut lying halfway between septum and lateral wall, the center of the ventricular cavity, radius of search, and the most apical point to align to the 90° arc. From that point on, CPs for each long-axis cut were generated automatically from the most septal to the most lateral cuts. This procedure was performed for each stress and each delayed tomographic study. Percent washout CPs were then calculated as the stress profile minus the delayed profile, multiplied by 100 over the stress profile, using the profiles of the corresponding anatomic cut at stress and delayed tomography, respectively.

After all of the long- and short-axis circumferential profiles had been extracted, they were mapped into a two-dimensional (2D) polar representation. In this mapping (Fig. 2), the apex corresponds to the center of the polar representation and the outermost circle corresponds to the most basal cut that was processed. The arcs between 60° to 120° of each long-axis cut are mapped into the central region of the display to depict the apical Tl-201 distribution. Immediately surrounding the apical region, the entire (0° to 360°) most apical short-axis stress profile is mapped with all of the following short-axis CPs being mapped in increasingly larger circles until the most basal CP is reached. In this representation the sector from 315° to 60° is assigned to the area perfused by the left circumflex coronary artery, 60°–120° to the right coronary, and 120°–315° to the left anterior descending. In the 2D polar map, the size of the display always remains the same, so the size of the LV is reflected by the number of CPs that are mapped. Thus in larger LVs, the band representing each slice is thinner relative to smaller LVs. A similar 2D polar map representation is then generated using washout CPs instead of stress CPs.

Definition of normal limits

In order to account for variation in LV size, the ventricle was divided into anatomic regions. Five regions, of equal thickness, represented the volume displayed by the short-axis cuts, and five regions, of equal thickness, represented the volume displayed by the long-axis cuts (Fig. 3). The mean value and standard deviation were established from the pooled data of 20 normal patients (Group A) for each of the 60 angular locations of each of the five anatomic regions corresponding to the short-axis and long-axis cuts. The times at which the stress image and redistribution image were obtained was used to interpolate the CPs from the delayed tomograms and washout CPs to exactly 4 hr in the same manner as in our planar approach (*8*).

For the distribution profiles, normal limits were defined as the curves representing 2.5 standard deviations (s.d.) below the mean, and were used as the threshold for defect detection. These curves were obtained by averaging the profiles corresponding to each anatomic region, point by point, around the circumference of the myocardium and calculating the standard deviation for each point. Similarly for the washout profiles the normal limits for the 4-hr percent washout were defined from curves representing 2.5 s.d. below the mean for those intervals. Thus ten circumferential profiles corresponding to lower limits of normal of the short- and long-axis anatomic regions were generated for the stress distribution, and ten for the percent-washout circumferential profiles. The criterion of defining the normal limits at 2.5 s.d. below the mean was used for two reasons: the set of circumferential profiles from the normal patients did not form a Gaussian distribution, and this value resulted in an optimal tradeoff between sensitivity and specificity for detecting coronary artery disease using our previously developed quantitative Tl-201 planar approach (*16*).

Quantitative interpretation

Initial distribution and washout circumferential profiles for the 25 normals and the 28 patients with CAD were interpreted by a computer program that aligned the curves, determined the anatomic region where each profile belonged, and compared each curve with the empirically determined normal limits (described above) corresponding to the profile's anatomic region. The normal limits for the 4-hr percent washout were corrected to the actual imaging time (3–6 hr) as described previously (*8*).

In order to quantify the three-dimensional involve-

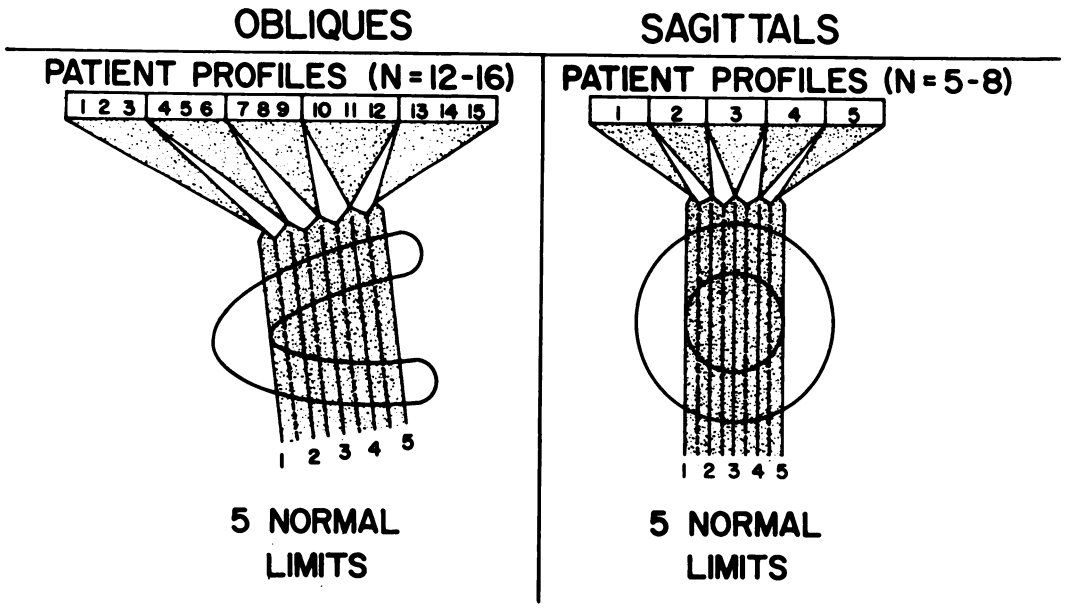

FIGURE 3
Method for dividing left ventricle into 5 anatomic short-axis (oblique) regions (left) and 5 long-axis (sagittal) regions (right). This division is performed for both development of profiles for normal limits and for assignment of which normal-limit profile will be used in assessing circumferential profile extracted from specific cut. This example illustrates assignment of anatomic regions in patient with 15 short-axis and 5 long-axis cuts

ment of an abnormality, two types of polar maps were generated: one for the extent of an abnormality and the other for its severity. These two kinds of maps were generated for both the initial distribution and the 4-hr washout of Tl-201. In the extent polar map, the CPs are compared with the lower limit of normal generated for that region. Those points falling below normal are set to zero and the remaining points are set to one. Thus the extent map is a binary map where the fraction of abnormal myocardium is computed as the percentage of LV pixels that are set to zero. In the severity map, the pixels representing the polar map are shown as a gray level between black and white depending on the degree of the abnormality. The value of each pixel is computed such that if the pixel is above normal limits it gets a value of 1. If below, it gets a fractional value linearly dependent on how far it falls below the normal limit. We termed this value a point score.

Various quantitative criteria for abnormality were applied to the subjects in Groups A and B, and the criteria that best separated the normals from the patients with CAD were defined. The following criteria for abnormality of the polar maps were evaluated.

1. In the extent map of the stress distribution, the percentage of pixels indicating low uptake.
2. In the extent map of the percent washout distribution, the percentage of pixels indicating slow washout.
3. In the severity map of the stress distribution, the point score for low uptake.
4. In the severity map of the percent washout distribution, the point score for slow washout.

Two different sets of criteria were determined, the first for overall presence or absence of CAD, and the second for presence of abnormality in the territories of either the anterior or posterior coronary circulation. The anterior circulation territory was represented by the sector in the polar map extending from 120° to 315°, while that of the posterior circulation occupied the remaining portion of the myocardium. The apical region, although used for overall detection of disease, was not assigned to either the anterior or posterior circulation.

RESULTS

Results in normals

The normal stress-distribution and washout characteristics of three of the five anatomic short-axis regions of the LV, and their associated standard deviations above and below the normal mean curve, are shown in Fig. 4. The mean stress distribution profiles at different depths of the LV show that radiation originating from the inferior and septal regions is attenuated more than that from the anterior and lateral walls. Differential attenuation is even more pronounced in the basal tomograms, as suggested by increased interregional count difference and widening of the standard deviation. The mean myocardial washout profiles at 4 hr demonstrate little change between the different LV depths, and a uniform percent washout rate of 48%. This indicates that the percent washout rate is not affected by attenuation, since

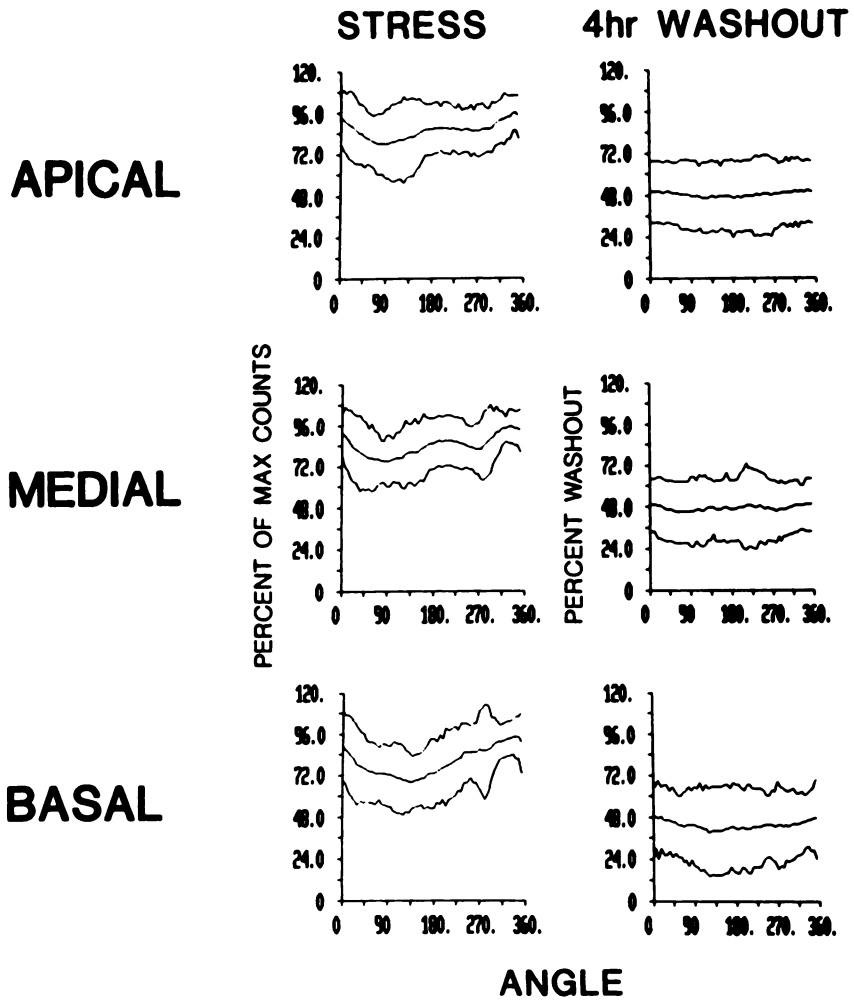

FIGURE 4
Circumferential profiles for stress distribution and 4-hr washout representing mean ± 2.5 s.d. from three of anatomic oblique short-axis cuts in group of 20 normal patients. Note reduced lower limits of normal stress-distribution profiles approximately between 45°–225°, corresponding to inferior and septal regions of myocardium. This reduction is partially due to increased scatter and attenuation experienced by photons from these regions. Note also increased reduction in adjacent regions going from apex to base

it represents temporal changes in regional Tl-201 concentration. Furthermore, all portions of the normal myocardium lose Tl-201 at essentially the same rate.

Criteria for detection and localization of CAD

In the patients studied the distribution of perfusion defect sizes ranged from no abnormality to 64% of the myocardium abnormal. The mean defect size was 26%, with a standard deviation of 19%. For extent of abnormality, the criteria that best separated normals from the patients with CAD were determined in terms of the percentage of the LV myocardium that must be abnormal to qualify for a true abnormality. Table 1 illustrates the effect of varying criteria for the extent of abnormality on the true positive and negative rates. A cutoff criterion of perfusion defects greater than or equal to 3% of the myocardium was selected as providing the best tradeoff between true-positive and true-negative rates. This resulted in the correct detection of the presence or absence of disease in 23 of 25 normals and 25 of the 28 CAD patients. Similarly, criteria for abnormality in the circulation territory of either coronary were determined from the percentage of abnormality in that region that was required for true abnormality. Table 2 illustrates the effect of varying criteria for the extent of myocardium abnormality on the true-positive and true-negative rates for disease in each circulation. Perfusion defects greater than or equal to 5% of the anterior myocardial region and 16% of the posterior region were selected as providing the best tradeoff between true-positive and true-negative rates. These criteria resulted in the correct localization of the presence or absence of disease in 18 of 20 diseased and seven of eight normal anterior circulation territories and in 16 of 22 diseased and five of six normal posterior circulation territories. Criteria for washout abnormalities (Tables 1 and 2), or for the severity of disease (point

TABLE 1
Effect of Varying Criteria for Extent of Myocardium Abnormal on True-Positive and True-Negative Rates for Detection of Coronary Disease

% Myocardium abnormal (≥)	Criteria: Perfusion defect 10	5	3*	% Washout abnormality 10	5	3
% True positive (n = 26)	71	82	89	57	64	75
% True negative (n = 25)	100	100	92	96	96	92

* Selected as optimal criterion.

score) did not further discriminate CAD patients from normals, or better ascribe disease to the anterior or posterior circulation. Characteristic examples of the results obtained in a patient with CAD are illustrated in Figs. 5 through 7.

Interobserver agreement

Stress-redistribution Tl-201 rotational tomography from ten patients, seven with and three without CAD, were analyzed by two independent computer operators. Each extent map was divided into an anterior and a posterior region. Using the criteria described above, the stress perfusion and washout three-dimensional distributions were analyzed to determine whether abnormality was present and, if so, whether it involved the anterior and/or posterior coronary circulation. Concordance was obtained in all ten patients and in all 20 segments.

DISCUSSION

It has been our experience (*17,18*) and that of others (*9–12*) that quantitative analysis of planar images (*9–12*) and seven-pinhole tomograms (*11,19*) significantly enhances the diagnostic accuracy of Tl-201 myocardial scintigraphy over that of visual interpretation. Furthermore, we recently compared visual interpretation of rotational tomograms with qualitative analysis of planar scintigraphy, and although we found no difference in the sensitivity of detecting CAD, we did find that tomography better identified the location of disease (*2*). We anticipate that quantification of Tl-201 rotational tomography will not only enhance its diagnostic accuracy but also may allow for the determination of the percentage of the myocardium involved with abnormal perfusion, a measurement recognized to be clinically important (*7,20–22*), particularly when Tl-201 studies are used for prognosis. Quantification should also allow for the objective comparison between the different Tl-201 modalities.

The present investigation utilizes the attributes of our previously described method of quantifying planar images and describes a specific protocol for selecting appropriate tomograms for quantification. It also describes a method for incorporating circumferential profiles of the short- and long-axis cross sections into a comprehensive display that expresses the three-dimensional stress distribution and percent washout in two-dimensional polar coordinates.

This method of space/time quantification of the three-dimensional Tl-201 distribution is comprehensive, utilizing a computer to (a) acquire and correct for nonuniformity of the projections, (b) reconstruct the transaxial, sagittal, and oblique tomograms, (c) extract the maximal-count circumferential profile for each short- and long-axis cut selected, (d) calculate for each cut the circumferential profile for percent washout, (e) compare each patient's profiles with previously established normal limits, (f) synthesize all of the profiles into a comprehensive polar display of the Tl-201 distributions for stress and 4-hr percent washout, and (g) express the extent and severity of perfusion abnormalities.

The acquisition of the 32 projections was performed using the 180° rather than the 360° collection method in order to obtain higher image contrast and resolution (*6,23,24*). This investigation did not inquire whether the redistribution that occurred during the 20 min of post-stress acquisition influenced our results. Nevertheless, MacIntyre (*25*) and Kirsch (*26*) have reported from preliminary observations that this redistribution did not

TABLE 2
Effect of Varying Criteria for Extent of Myocardium Abnormal on True-Positive and True-Negative Rates for Localization of Coronary Disease

Anterior Circulation (LAD)

% Myocardium abnormal (≥)	Criteria: Perfusion defect 20	10	5*	% Washout abnormality 20	10	5
% True positives (n = 19)	75	80	90	65	65	65
% True negatives (n = 7)	88	88	88	88	88	88

Posterior circulation (RCA, LCX)

% Myocardium abnormal (≥)	Criteria: Perfusion defect 30	16*	10	% Washout abnormality 20	10	5
% True positives (n = 21)	50	73	82	41	55	73
% True negatives (n = 5)	100	83	50	83	83	83

* Selected as optimal criterion.

ERRATUM: Please replace this corrected page with the original that appeared in the January 1985 issue. The printer regrets any inconvenience thus caused.

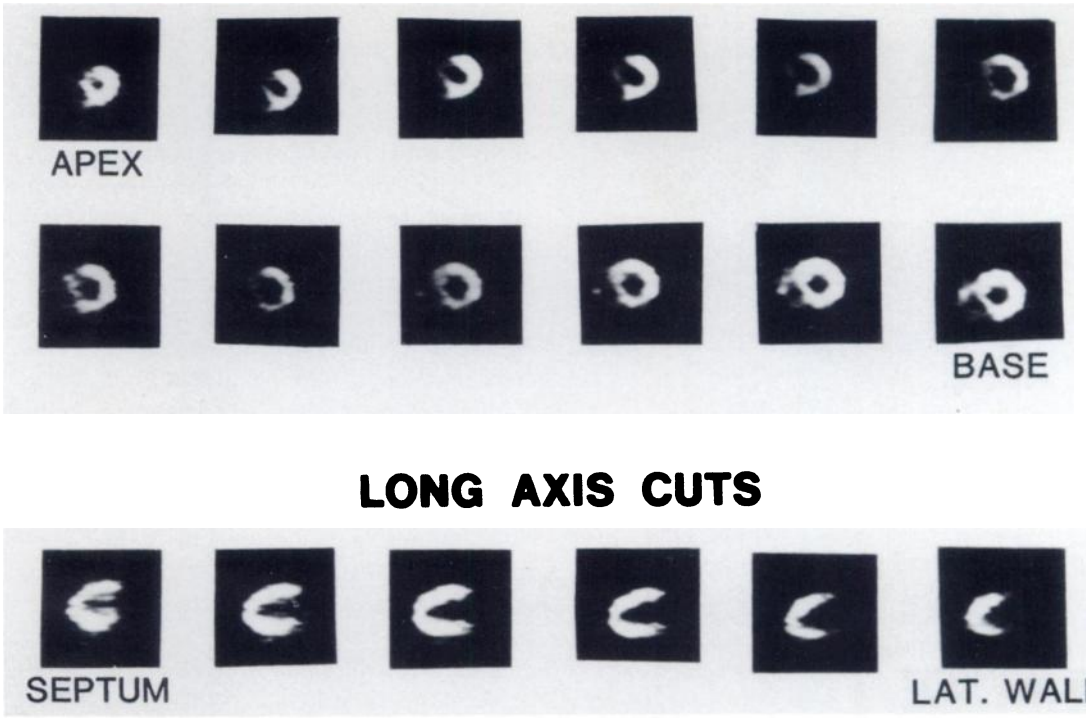

FIGURE 5
Stress Tl-201 myocardial short- and long-axis cuts in patient with a 90% stenosis of left anterior descending coronary artery, located immediately after first diagonal branch. Note perfusion defects evident in short-axis cuts approximately from 8 to 11 o'clock

appear to have a significant effect on their results. The tomograms were reconstructed without correction for scattering or attenuation, due to the difficulties involved in correcting for the variable attenuation of 80-keV x-rays through the thorax. Without such corrections, which demand 360° sampling, absolute quantification of the Tl-201 regional concentration is not possible, i.e., a voxel value will not be directly proportional to the concentration of Tl-201 occupying that unit volume. Furthermore, without this correction the appearance of the myocardium and abnormalities can be somewhat distorted (*23*,*27*). Nevertheless our approach, comparing the regional Tl-201 distribution with the corresponding lower limits of normal, partly compensated for this problem. This compensation is evidenced by the fact that—despite the appearance in normals of reduced counts in the more basal portions of the septal and inferior walls—none were considered abnormal after comparison of the profiles with the lower limits of normal. This compensation should allow a clinically useful degree of accuracy for the calculation of the percentage of abnormal area of the myocardium from the extent maps, and particularly from the severity maps. Nevertheless, without a 360° geometry and without correction for attenuation and scatter, the data reported in this paper are limited for purposes of absolute quantification.

Our method used the comparison of patient profiles with normal limits determined from patients having less than 5% likelihood of disease, based on sequential Bayesian analysis (*8*,*13*,*17*). This approach avoids the pitfalls of using patients with normal coronary arteriograms who may have nonatherosclerotic ischemic disease (*28*). Furthermore, it allows the use of age-matched controls, which if attempted with "normal volunteers," might result in inclusion of an unacceptable proportion of patients with occult coronary disease.

In our method, we extracted the entire three-dimensional myocardial Tl-201 distribution by analyzing the apex from the long-axis cuts and the rest of the myocardium from the short-axis cuts. We selected only slices that contained the ventricular cavity and thus clearly included the myocardium along the entire thickness of cut. An advantage of this approach is that it avoids the problem of the partial-volume effect of sampling only a portion of a wall. Another advantage is that it allows comparison of corresponding myocardial regions from stress to redistribution, since the depth of the tomographic planes is referenced to the subendocardial aspect of the apex on both stress and redistribution tomograms.

The analysis of myocardial Tl-201 washout did not result in any added detection or localization of disease. This is partly to be expected, since the mechanism for improved detection and localization of disease in planar

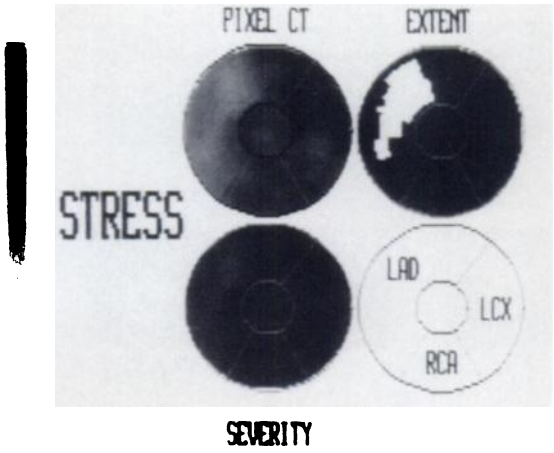

FIGURE 6
Two-dimensional polar representations of Tl-201 myocardial stress distribution for CAD patient illustrated in Fig. 5. Top left map (PIXEL CT) represents three-dimensional myocardial count distribution, ranging from black (high counts) to light gray (low counts). White region in extent map corresponds to locations where circumferential profiles fall below normal limits. Severity map shows how far below normal each of those locations fell. Display at lower right illustrates how regions have been assigned to specific coronary arteries. Note that perfusion defect shown in extent map falls in region supplied by LAD

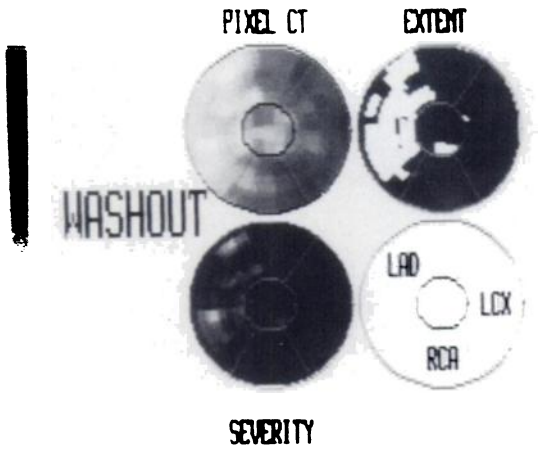

FIGURE 7
Two-dimensional polar representations of Tl-201 myocardial 4-hr percent washout of CAD patient illustrated in Figs. 5 and 6. Top left map represents three-dimensional percent washout distribution, ranging from black (faster washout) to light gray (slower washout). Note that white region in extent map, representative of abnormally slow washout, corresponds to region supplied by LAD

imaging by washout analyses depends on the lower contrast resolution of perfusion defects due to the overlap of diseased and normal myocardium. Nevertheless, further investigation may show that analysis of myocardial washout from myocardial tomograms could prove to be an important tool for separating ischemic from infarcted myocardium.

The accuracy for the percentage of abnormal myocardium is somewhat affected by cardiac and thoracic motion. This motion has been reported to account for overestimation of defect activity when infarct size (*29*) or myocardial blood flow are quantified (*30*). This has also been reported by Kirsch (*26*) to be responsible for false-negative results in patients with small hearts having high ejection fractions or hypertrophy. Kirsch also reported cardiac motion to result in false-positive findings in large hypertrophic hearts and in patients with cardiomyopathy. The distortion caused by motion is nevertheless thought to be small relative to that caused by attenuation and scatter. The accuracy for the percentage of abnormal myocardium is also affected by the system's spatial resolution (*31*). Hoffman (*31*) has shown that there is a significant reduction in the reconstructed voxel value for objects smaller than twice the FWHM of the spatial resolution, with this reduction increasing with decreasing object size. These results have been verified by Keyes (*29*) for infarct sizing and by Caldwell (*30*) for measurements of blood flow. It is likely that this dependence on the system's spatial resolution would tend to mask small nontransmural perfusion defects while it overestimates the size of transmural defects.

With respect to sizing of perfusion defects, Tamaki et al. (7) measured infarct volume by applying manual computer planimetry of the normal and infarcted regions to tomographic cross sections. This approach was compared with similar measurements using planar Tl-201 scintigraphy for its ability to correlate with the accumulated creatine kinase-MB (CK-MB) isoenzyme release. In spite of the limitations of Tl-201 tomography described above, they found a better correlation with CK-MB release using manual computer planimetry of the reconstructed tomograms than with planar measurements.

An advantage of our approach over that of Tamaki is its greater degree of objectivity of the measurements. The method presented showed excellent interobserver agreement for the detection and localization of the perfusion abnormalities, thus indicating a high degree of reproducibility. This important attribute is to be expected of an objective computerized method, particularly since there is a specific protocol for selecting the tomograms to be reconstructed and since the stress distribution and washout abnormalities are automatically detected and sized by the computer. The method also circumvented the problems associated with the partial volume effect by processing the selected tomograms that clearly included the myocardium along the entire thickness of the cut.

Some limitations of the approach described here should be noted. One disadvantage is that it gives equal weights to the contribution of small and large slices. In

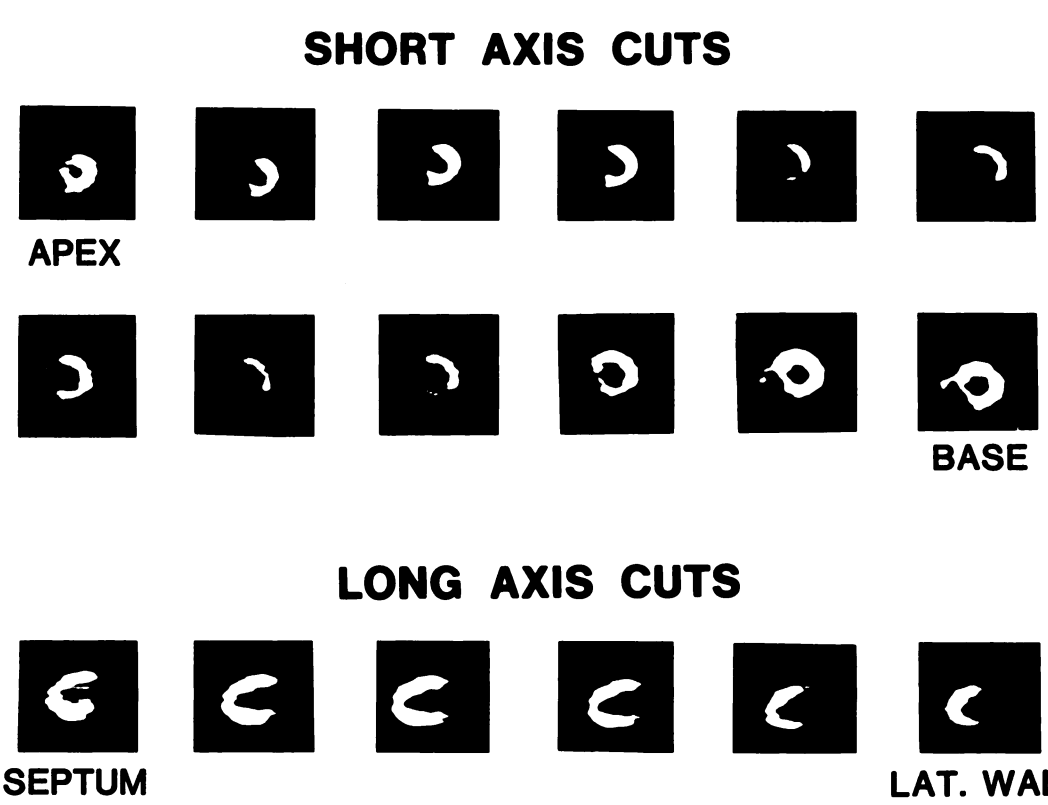

FIGURE 5
Stress Tl-201 myocardial short- and long-axis cuts in patient with a 90% stenosis of left anterior descending coronary artery, located immediately after first diagonal branch. Note perfusion defects evident in short-axis cuts approximately from 8 to 11 o'clock

thickness of the cut.

Some limitations of the approach described here should be noted. One disadvantage is that it gives equal weights to the contribution of small and large slices. In appear to have a significant effect on their results. The tomograms were reconstructed without correction for scattering or attenuation, due to the difficulties involved in correcting for the variable attenuation of 80-keV x-rays through the thorax. Without such corrections, which demand 360° sampling, absolute quantification of the Tl-201 regional concentration is not possible, i.e., a voxel value will not be directly proportional to the concentration of Tl-201 occupying that unit volume. Furthermore, without this correction the appearance of the myocardium and abnormalities can be somewhat distorted (*23,27*). Nevertheless our approach, comparing the regional Tl-201 distribution with the corresponding lower limits of normal, partly compensated for this problem. This compensation is evidenced by the fact that—despite the appearance in normals of reduced counts in the more basal portions of the septal and inferior walls—none were considered abnormal after comparison of the profiles with the lower limits of normal. This compensation should allow a clinically useful degree of accuracy for the calculation of the percentage of abnormal area of the myocardium from the extent maps, and particularly from the severity maps. Nevertheless, without a 360° geometry and without correction for attenuation and scatter, the data reported in this paper are limited for purposes of absolute quantification.

Our method used the comparison of patient profiles with normal limits determined from patients having less than 5% likelihood of disease, based on sequential Bayesian analysis (*8,13,17*). This approach avoids the pitfalls of using patients with normal coronary arteriograms who may have nonatherosclerotic ischemic disease (*28*). Furthermore, it allows the use of age-matched controls, which if attempted with "normal volunteers," might result in inclusion of an unacceptable proportion of patients with occult coronary disease.

In our method, we extracted the entire three-dimensional myocardial Tl-201 distribution by analyzing the apex from the long-axis cuts and the rest of the myocardium from the short-axis cuts. We selected only slices that contained the ventricular cavity and thus clearly included the myocardium along the entire thickness of cut. An advantage of this approach is that it avoids the problem of the partial-volume effect of sampling only a portion of a wall. Another advantage is that it allows comparison of corresponding myocardial regions from stress to redistribution, since the depth of the tomographic planes is referenced to the subendocardial aspect of the apex on both stress and redistribution tomograms.

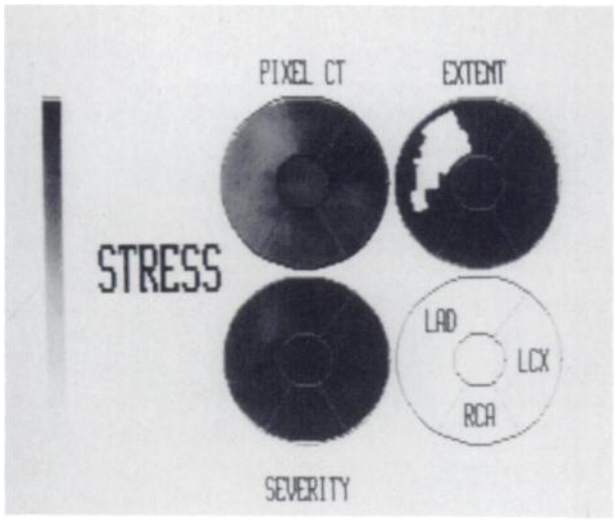

FIGURE 6
Two-dimensional polar representations of Tl-201 myocardial stress distribution for CAD patient illustrated in Fig. 5. Top left map (PIXEL CT) represents three-dimensional myocardial count distribution, ranging from black (high counts) to light gray (low counts). White region in extent map corresponds to locations where circumferential profiles fall below normal limits. Severity map shows how far below normal each of those locations fell. Display at lower right illustrates how regions have been assigned to specific coronary arteries. Note that perfusion defect shown in extent map falls in region supplied by LAD

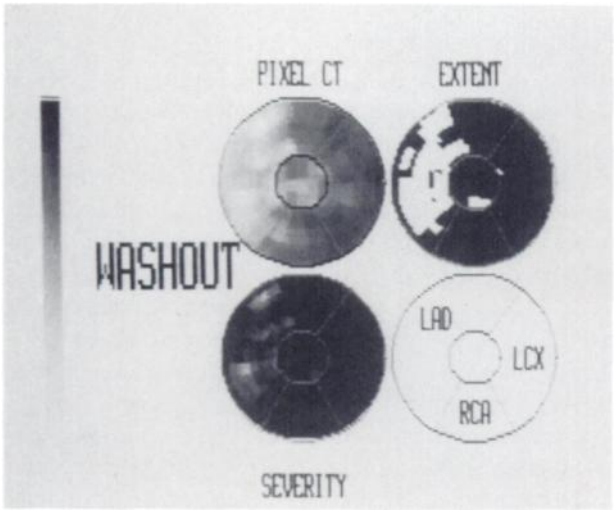

FIGURE 7
Two-dimensional polar representations of Tl-201 myocardial 4-hr percent washout of CAD patient illustrated in Figs. 5 and 6. Top left map represents three-dimensional percent washout distribution, ranging from black (faster washout) to light gray (slower washout). Note that white region in extent map, representative of abnormally slow washout, corresponds to region supplied by LAD

The analysis of myocardial Tl-201 washout did not result in any added detection or localization of disease. This is partly to be expected, since the mechanism for improved detection and localization of disease in planar imaging by washout analyses depends on the lower contrast resolution of perfusion defects due to the overlap of diseased and normal myocardium. Nevertheless, further investigation may show that analysis of myocardial washout from myocardial tomograms could prove to be an important tool for separating ischemic from infarcted myocardium.

The accuracy for the percentage of abnormal myocardium is somewhat affected by cardiac and thoracic motion. This motion has been reported to account for overestimation of defect activity when infarct size (*29*) or myocardial blood flow are quantified (*30*). This has also been reported by Kirsch (*26*) to be responsible for false-negative results in patients with small hearts having high ejection fractions or hypertrophy. Kirsch also reported cardiac motion to result in false-positive findings in large hypertrophic hearts and in patients with cardiomyopathy. The distortion caused by motion is nevertheless thought to be small relative to that caused by attenuation and scatter. The accuracy for the percentage of abnormal myocardium is also affected by the system's spatial resolution (*31*). Hoffman (*31*) has shown that there is a significant reduction in the reconstructed voxel value for objects smaller than twice the FWHM of the spatial resolution, with this reduction increasing with decreasing object size. These results have been verified by Keyes (*29*) for infarct sizing and by Caldwell (*30*) for measurements of blood flow. It is likely that this dependence on the system's spatial resolution would tend to mask small nontransmural perfusion defects while it overestimates the size of transmural defects.

With respect to sizing of perfusion defects, Tamaki et al. (7) measured infarct volume by applying manual computer planimetry of the normal and infarcted regions to tomographic cross sections. This approach was compared with similar measurements using planar Tl-201 scintigraphy for its ability to correlate with the accumulated creatine kinase-MB (CK-MB) isoenzyme release. In spite of the limitations of Tl-201 tomography described above, they found a better correlation with CK-MB release using manual computer planimetry of the reconstructed tomograms than with planar measurements.

An advantage of our approach over that of Tamaki is its greater degree of objectivity of the measurements. The method presented showed excellent interobserver agreement for the detection and localization of the perfusion abnormalities, thus indicating a high degree of reproducibility. This important attribute is to be expected of an objective computerized method, particularly since there is a specific protocol for selecting the tomograms to be reconstructed and since the stress distribution and washout abnormalities are automatically detected and sized by the computer. The method also circumvented the problems associated with the partial volume effect by processing the selected tomograms that clearly included the myocardium along the entire

order to measure the size of perfusion defects accurately by our approach, we need to account for the differences in myocardial mass contributed by slices of different sizes and different endocardial-to-epicardial thicknesses. Furthermore, in order to relate the defect size accurately to the total LV mass, we need to incorporate the mass from the three basal slices, which we are not currently analyzing. Our method of calculating the severity of abnormality through the use of the point score should become increasingly significant with the incorporation of an accounting for the true LV mass. It should be emphasized that without corrections for scattering, attenuation, object size, heart motion, and myocardial thickness, the error of measuring infarct size or perfusion defect size could be considerable.

This paper is intended to describe our method fully and to provide preliminary criteria from pilot groups of normal patients and patients with CAD. In our pilot population, the method proved to be accurate in separating normal patients from those with CAD, and in localizing anterior and posterior disease. Our method for determining the criteria for abnormality of each vascular territory was empirical. We found that a significantly larger perfusion defect was required as a criterion for localizing disease to the posterior circulation compared with the anterior. This difference is likely due to the inherently smaller standard deviation of the posterior circulation territory, which is less affected by attenuation. We should emphasize that the criteria that best separated normals from patients with CAD, and best distinguished anterior from posterior disease, are preliminary. A larger prospective evaluation is needed, in which these criteria are applied to assess sensitivity and specificity for detection of CAD and for ascribing disease to the anterior and posterior coronary circulations. In this evaluation we are comparing the percentage of abnormal area, as determined from the extent and severity maps with the severity of CAD as determined from quantitative analysis of coronary arteriography. We find that both the lower limits of normal profiles and the criteria described above are considerably affected by the exact methods of acquisition, preprocessing, reconstruction and quantification. We foresee that any improvements to our method will necessarily have to be accompanied by the establishment of new normal limits and criteria.

This new, comprehensive computerized method offers promise to provide accurate, objective, reproducible, quantitative assessment of the three-dimensional relative stress distribution and washout characteristics of thallium-201 in the myocardium. Furthermore, it offers the potential to quantify the percent of the abnormally perfused myocardium. In patients with coronary artery disease this measurement may well be an important indicator of long-term prognosis, and thus a highly useful parameter for guiding patient management.

ACKNOWLEDGMENTS

The authors gratefully acknowledge the development and performance of acquisition protocols by James Bietendorf, the research assistance of Jan Nielsen, Ana Becerra, and Chris Wong, and the technical assistance of Greg Kuhl and Lance Laforteza.

This work was supported in part by Specialized Center of Research (SCOR) Grant No. HL-17651 from the National Heart, Lung, and Blood Institutes, NIH, Bethesda, Maryland, and by Grants from the American Heart Association, Greater Los Angeles Affiliate, Inc. The work was presented in part at the 30th Annual Meeting of the Society of Nuclear Medicine in St. Louis, Missouri.

REFERENCES

1. Go RT, Cook SA, MacIntyre WJ, et al: Comparative accuracy of stress and redistribution thallium-201 cardiac single photon emission transaxial tomography and planar imaging in the diagnosis of myocardial ischemia. *J Nucl Med* 23:P25, 1982 (abstr)
2. Prigent F, Friedman J, Maddhai J, et al: Comparison of rotational tomography with planar imaging for thallium-201 stress myocardial scintigraphy. *J Nucl Med* 24:P18, 1983 (abstr)
3. Tamaki N, Yonekura Y, Mukai T, et al: Values and limitations of segmental analysis of stress and redistribution Tl ECT for location of coronary artery disease. *J Nucl Med* 24:P18, 1983 (abstr)
4. Mortelmans L, De Roo M, Devos P, et al: Segmental analysis of Tl-201 emission computerized tomography of the heart. Evaluation by coronarographic data. *J Nucl Med* 23:P25, 1982 (abstr)
5. Maublant J, Cassagnes J, LeJeune JJ, et al: A comparison between conventional scintigraphy and emission tomography with thallium-201 in the detection of myocardial infarction: Concise communication. *J Nucl Med* 23:204–208, 1982
6. Ritchie JL, Williams DL, Harp G, et al: Transaxial tomography with thallium-201 for detecting remote myocardial infarction. *Am J Cardiol* 50:1236–1241, 1982
7. Tamaki S, Nakajima H, Murakami T, et al: Estimation of infarct size by myocardial emission computed tomography with thallium-201 and its relation to creatine kinase-MB release after myocardial infarction in man. *Circulation* 66(5):994–1001, 1982
8. Garcia E, Maddahi J, Berman DS, et al: Space/time quantitation of thallium-201 myocardial scintigraphy. *J Nucl Med* 22:309–317, 1981
9. Watson DD, Campbell NP, Read EK, et al: Spatial and temporal quantitation of planar thallium myocardial images. *J Nucl Med* 22:577–584, 1981
10. Meade RC, Bamrah VS. Horgan JD, et al: Quantitative methods in the evaluation of thallium-201 myocardial perfusion images. *J Nucl Med* 19:1175–1178, 1978
11. Vogel RA, Kirch DL, LeFree MT, et al: Thallium-201 myocardial perfusion scintigraphy: Results of standard and multi-pinhole tomographic techniques. *Am J Cardiol* 43:787–793, 1979
12. Burow RD, Pond M, Schafer AW, et al: "Circumferential profiles:" A new method for computer analysis of thallium-201 myocardial perfusion images. *J Nucl Med* 20:771–777, 1979

13. Diamond GA, Forrester JS: Analysis of probability as an aid in the clinical diagnosis of coronary artery disease. *N Engl J Med* 300:1350-1358, 1979
14. Areeda J, Chapman D, Van Train K, et al: Methods for characterizing and monitoring rotational gamma camera system performance. In *Emission Computed Tomography: Current Trends.* Esser PD, ed. New York, Society of Nuclear Medicine, 1983, pp 81-90
15. Borrello JA, Clinthorne NH, Rogers WL, et al: Oblique-angle tomography: A restructuring algorithm for transaxial tomographic data. *J Nucl Med* 22:471-473, 1981
16. Van Train K, Garcia E, Maddahi J, et al: Improved quantitation of stress/redistribution Tl-201 scintigrams and evaluation of normal limits. In *Computers in Cardiology, IEEE Computer Society*, 1982, pp 311-314
17. Maddahi J, Garcia EV, Berman DS, et al: Improved noninvasive assessment of coronary artery disease by quantitative analysis of regional stress myocardial distribution and washout of thallium-201. *Circulation* 64:924-935, 1981
18. Bateman T, Garcia E, Maddahi J, et al: Clinical evaluation of seven-pinhole tomography for the detection and localization of coronary artery disease: Comparison with planar imaging using quantitative analysis of myocardial thallium-201 distribution and washout after exercise. *Am Heart J* 106:263-271, 1983
19. Francisco DA, Collins SM, Go RT, et al: Tomographic thallium-201 myocardial perfusion scintigrams after maximal coronary artery vasodilation with intravenous dipyridamole. Comparison of qualitative and quantitative approaches. *Circulation* 66:370-379, 1982
20. Wackers FJT, Becker AE, Samson G, et al: Location and size of acute transmural myocardial infarction estimated from thallium-201 scintiscans: a clinicopathological study. *Circulation* 56:72-78, 1977
21. Niess GS, Logic JR, Russell RO, et al: Usefulness and limitations of thallium-201 myocardial scintigraphy in delineating location and size of prior myocardial infarction. *Circulation* 59:1010-1019, 1979
22. Morrison J, Coromilas J, Munsey D, et al: Correlation of radionuclide estimates of myocardial infarction size and release of creatine kinase-MB in man. *Circulation* 62:277-289, 1980
23. Tamaki N, Mukai T, Ishii Y, et al: Comparative study of thallium emission myocardial tomography with 180° and 360° data collection. *J Nucl Med* 23:661-666, 1982
24. MacIntyre WJ, Go RT, Hauser TS, et al: Evaluation of 180-Deg and 360-Deg reconstruction of the heart by transaxial tomography with thallium-201. In *Digital Imaging*, Esser PD, ed. New York, Society of Nuclear Medicine, 1982, pp 197-203
25. MacIntyre WJ, Go RT, Cook SA, et al: Comparison of stress and redistribution thallium-201 planar imaging with a single photon transaxial tomographic technique. In *Nuclear Medicine and Biology, Proceedings of the Third World Congress of Nuclear Medicine and Biology.* Raynaud C, ed. Paris, Pergamon, 1982, pp 1281-1284
26. Kirsch C-M, Doliwa R, Buell U, et al: Detection of severe coronary heart disease with Tl-201: Comparison of resting single photon emission tomography with invasive arteriography. *J Nucl Med* 24:761-767, 1983
27. Hoffman EJ: 180° compared with 360° sampling in SPECT. *J Nucl Med* 23:745-747, 1982
28. Berger BC, Watson DD, Burwell LR, et al: Redistribution of thallium at rest in patients with stable and unstable angina and the effect of coronary artery bypass surgery. *Circulation* 60:1114-1125, 1979
29. Keyes JW, Leonard PF, Brody SL, et al: Myocardial infarct quantification in the dog by single photon emission computed tomography. *Circulation* 58:227-232, 1978
30. Caldwell JH, Williams DL, Hamilton GW, et al: Regional distribution of myocardial blood flow measured by single-photon tomography: Comparison with in vitro counting. *J Nucl Med* 23:490-495, 1982
31. Hoffman EJ, Huang SC, Phelps ME: Quantitation in positron emission computed tomography. 1. Effect of object size. *J Comput Assist* 3:299-308, 1979